Proceedings of ASME Turbo Expo 2011
GT2011
June 6-10, 2011, Vancouver, British Columbia, Canada

GT2011-46498

TURBULENCE AND HEAT TRANSFER MEASUREMENTS IN AN INCLINED LARGE SCALE FILM COOLING ARRAY – PART II, TEMPERATURE AND HEAT TRANSFER MEASUREMENTS

Douglas R. Thurman
US Army Research Laboratory
Glenn Research Center
Cleveland, Ohio, USA

Lamyaa A. El-Gabry
Mechanical Engineering Department
The American University in Cairo
New Cairo, Egypt

Philip E. Poinsatte, James D. Heidmann
Turbomachinery and Heat Transfer Branch
NASA Glenn Research Center
Cleveland, Ohio, USA

ABSTRACT

The second of a two-part paper, this study focuses on the temperature field and surface heat transfer measurements on a large-scale models of an inclined row of film cooling holes. Detailed surface and flow field measurements were taken and presented in Part I. The model consists of three holes of 1.9-cm diameter that are spaced 3 hole diameters apart and inclined 30˚ from the surface. Additionally, another model with an anti-vortex adaptation to the film cooling holes is also tested. The coolant stream is metered and cooled to 20°C below the mainstream temperature. A thermocouple is used to obtain the flow temperatures along the jet centerline and at various streamwise locations. Steady state liquid crystal thermography is used to obtain surface heat transfer coefficients. Results are obtained for blowing ratios of up to 2 in order to capture off-design conditions in which the jet is lifted. Film cooling effectiveness values of 0.4 and 0.15 were found along the centerline for blowing ratios of 1 and 2 respectively. In addition, an anti-vortex design was tested and found to have improved film effectiveness. This paper presents the detailed temperature contours showing the extent of mixing between the coolant and freestream and the local heat transfer results.

INTRODUCTION

Turbine engine temperatures often exceed the material properties of metals used in engine components. A common method to protect the metal surface of blades from the hot gas temperatures in turbine engines is to use film cooling to keep a layer of cooler air over the surface of the material. Even though there are many studies on film cooling flows, there are many aspects of the interaction of the freestream and coolant flows that are not well understood or predicted computationally [1-3].

This study is the second of a two-part paper that provides high resolution experimental heat transfer and temperature data on a large scale model. The hole geometry (angle and pitch) is similar to that on the leading edge of a vane in a previous study described in Thurman et al [4]. Flow data with detailed velocity component and turbulence measurements are presented in Part I [5]. This paper describes the experimental heat transfer and temperature survey data for a large scale model that, when combined with the flow data, provides a set of high resolution data that will help validate computational heat transfer codes.

This paper will focus on film effectiveness, the temperature field, and the surface Nusselt number for an array of angled film cooling holes at a fixed density ratio at two blowing ratios. Film effectiveness on flat plate surfaces has been the focus of much research including the works including [6-9]. Foster et al. studied the effect of density and velocity ratio using a mass transfer analogy and showed the stream-wise variation of film effectiveness along the hole centerline [6] and also measured flow velocity and film effectiveness for varying inclination angles of 35, 55, and

90-degrees [7]. Sinha et al. [8] measured the film effectiveness at density ratios of 1.2 to 2.0 using surface mounted thermocouples and concluded that for detached jets, a consistent scaling was not found and for attached jets, the centerline effectiveness scaled with mass flux ratio. Kohli et al. [9] also studied film effectiveness for a flat plate geometry for 35 and 55 degree angles of injection at a density ratio of 1.6 and measured in addition to the adiabatic effectiveness the thermal and velocity field.

The thermal field has also been the focus of prior research [9, 10]. Thole et al. [10] measured the mean temperature profiles for a row of inclined jets for density ratio of 1.2 and 2.0 and found that the temperature field suggests that the coolant jet has three options: one is for the jet to remain attached to the surface, two is for the jet to detach and reattach and the third is for the jet to detach and remain detached from the surface. It is the third and to some extent the second case that present a challenge to film cooling turbine design and prediction and are the focus of the present research.

In addition to the flow temperature surveys and adiabatic film effectiveness results, the surface heat transfer is also an important aspect of film cooling that has been the subject of research studies. Dhungel et al. [11] use IR thermography to obtain detailed heat transfer and film effectiveness for a row of cylindrical film cooling holes, shaped holes, and a number of anti-vortex film cooling designs that incorporate side holes. The film holes are inclined at 30 degrees, spaced at 3 hole diameters and have a length of 4 hole-diameters. Yuen et al. [12] present heat transfer coefficients for film cooled surfaces with injection angles of 30, 60, and 90 degrees at blowing ratios ranging from 0.33 to 2 and conclude that the heat transfer results are less sensitive than the film effectiveness for the same conditions [13]. Goldstein [14] used the naphthalene sublimation technique to obtain heat transfer coefficients downstream of a row of 35-degree angled holes.

This study presents high resolution temperature field using thermocouple surveys and detailed local surface heat transfer data using liquid crystal thermography. The coolant used was air and was passed through an ice bath to chill and was fed through long tubes. Data was collected at various blowing ratios. In addition, centerline film effectiveness is reported. In the companion paper [5], the hydrodynamics is considered and velocity components and turbulence quantities are reported. The aim is to provide through the two papers a complete, detailed picture for code development and validation. A large L/D is used to approach conditions of fully developed flow at the ejection point in order to further facilitate code development in which it may not be therefore necessary to model the complexity of the plenum feed and one may be able to simply focus on the mainstream flow and jet interaction.

NOMENCLATURE

A	area of heater surface
D	diameter of film cooling hole
DR	jet to mainstream density ratio $= \rho_j / \rho_\infty$
H	heat transfer coefficient $= Q/[A \cdot (T_{lc} - T_{rec})]$
I	jet to mainstream momentum flux ratio $= \rho_j U_j^2 / \rho_\infty U_\infty^2$
k	thermal conductivity at freestream condition
L	length of film cooling hole
M	blowing ratio $= \rho_j U_j / \rho_\infty U_\infty$
Nu	Nusselt number $= HD/k$
Pr	Prandtl number
Q	heat supplied to the model
r	recovery factor $= Pr^{1/3}$
Re	Reynolds number based on hole diameter and inlet conditions
T_∞	mainstream inlet temperature
T_c	coolant temperature
U	velocity component in streamwise direction
U^*	normalized U-velocity = U/U_∞
VR	jet to mainstream velocity ratio $= U_j / U_\infty$
X	streamwise distance from hole leading edge
Y	spanwise distance from hole centerline
Z	vertical distance from tunnel floor (flat plate surface)
ρ	density
η	film effectiveness
θ	dimensionless air temperature

Subscripts

avg	average
j, c	jet or coolant
lc	liquid crystal
rec	recovery
rms	root mean square
s	static
t	total
∞	freestream (or mainstream) inlet

EXPERIMENTAL APPARATUS AND PROCEDURES

The test facility is shown in Figure 1. The tunnel consisted of an aluminum bellmouth, flow conditioning screens, square acrylic sections 8.2” wide and 0.75 inch (1.91 cm) thick, the test section on the floor of the tunnel and a lid directly above it for either viewing or actuator support. The tunnel was connected to a vacuum exhaust system which pulled room air through. The coolant flow was provided by blowing pressurized supply air through a heat exchanger, which consisted of a copper tube coiled inside an ice–water tank. The coolant was fed through a manifold to three separate flow meters, then through 45 cm of hose and 30 cm of acrylic tube, in an attempt to generate fully developed flow at the hole exit. The coolant flow path from flow meter to hole exit was nearly twice the required entrance length (L/D > 23 for the high blowing ratio case) for turbulent flow. The entire coolant path was insulated. The test section was a flat plate made of acrylic with three holes inclined at 30 degrees and a hole diameter of 1.9 cm (0.75 inch). The hole spacing was y/D = 3.

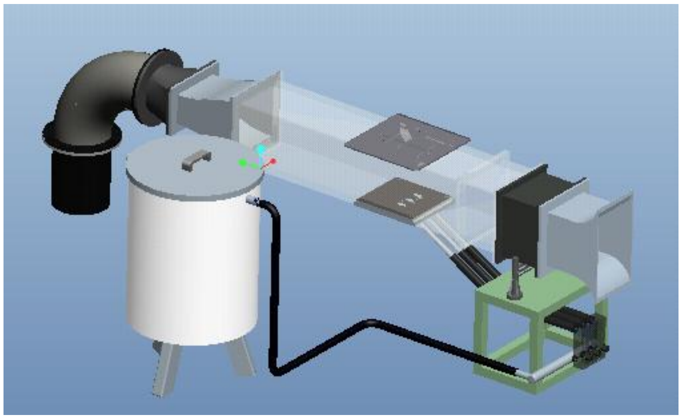

Fig 1. Test facility

For the heat transfer test, a second test section with matching geometry was employed. This section had a thin sheet of Inconel attached to the surface with double-sided tape downstream of the holes, with copper bus bars attached to the sides of the Inconel. A power supply was connected to the copper bus bars to provide a constant heat flux. Black paint and thermochromic liquid crystals were sprayed onto the plate.

A third model was tested employing an anti-vortex design similar to those of Heidmann [15]. This model was scaled similarly to the baseline three-hole model. It consisted of three large (.75 inch) holes at 30 deg incline but with two small (.25 inch) holes emanating from each main hole at an angle of 23 degrees. The coolant for this model was fed from an insulated plenum, however, rather than through 3 separate long tubes. Figure 2 shows the top view of both test sections with the different cooling hole designs.

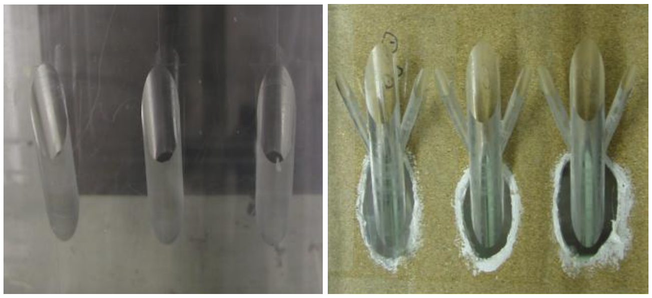

a) b)

Fig 2. Three cooling hole array at 30 deg incline:

a) Baseline model.

b) Anti-vortex model with 23 deg side holes fed from main hole.

To determine the tunnel flow rate, a total pressure probe was placed upstream of the test section and static pressure taps were placed on the sidewalls. The tunnel velocity was nominally 9 m/s. Freestream temperature was measured with an open-ball thermocouple located upstream of the holes near the total pressure probe. Coolant temperature was measured with open-ball thermocouples inside the coolant tubes. Temperature survey data was taken along the centerline plane of the tunnel and at several cross sectional planes with a (type E) thermocouple probe attached to an actuator above the test section. Results of the temperature surveys are non-dimensionalized using Equation [1]:

$$\theta = \frac{(T - T_\infty)}{(T_c - T_\infty)} \qquad [1]$$

Liquid crystals, by virtue of their ability to change color with temperature, provide a means to measure surface temperature and to visualize thermal patterns at any desired location. The liquid crystal paint was calibrated for color-temperature correspondence by using a thermocouple attached to the Inconel heater sheet. The yellow color isotherm was calibrated at 38 degrees C. A steady state method similar to that described in Russell et al [16] was used for heat transfer measurements. Electric power was supplied to the Inconel sheet and heated the surface. A color video camera captured the resulting temperature pattern produced by the liquid crystal. Surface heat transfer coefficients are calculated using Equation [2]:

$$H = \frac{Q}{A(T_{lc} - T_{rec})} \qquad [2]$$

The heat energy Q supplied to the heater sheet was calculated from the measured voltage across the Inconel foil and the current through a shunt resistor in series with the sheet. The area A is the measured area of the Inconel heater sheet. The temperature of the test surface T_{lc} was the calibrated liquid crystal temperature. The recovery temperature T_{rec} of the entrance freestream air is calculated using Equation [3]:

$$T_{rec} = T_s + r(T_t - T_s) \qquad [3]$$

A commercial video frame grabber was used to capture the heat transfer video data. The yellow calibrated color bands were digitized from the images. These digitized locations along with the heat flux measurements allowed for the calculation of heat transfer coefficients.

The film effectiveness is defined in Equation [4]:

$$\eta = \frac{(T_\infty - T_{aw})}{(T_\infty - T_c)} \qquad [4]$$

The adiabatic wall temperature was determined from the thermocouple probe surveys with the probe located near the floor of the test section.

EXPERIMENTAL RESULTS AND DISCUSSION

Thermocouple probe surveys were taken at nominal blowing ratios of 1 and 2 along the centerline of the tunnel and at various cross-sectional planes as shown in Figure 3, with higher resolution (0.254 mm) near the floor. An uncertainty analysis was performed on the flow and temperature measurements. Generally the flow data was nominally within 5% with most of this error from the relative low freestream velocity measurements. The uncertainty in temperature measurements ranged from 2% to 11% with the higher uncertainty at the very low theta values (< 0.10). Generally uncertainty values in the region of interest were conservatively estimated at under 5%.

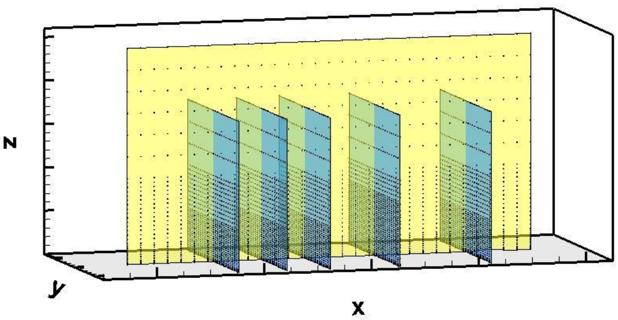

Fig 3. Survey planes for thermocouple probe

Figure 4 shows the temperature contours along the jet centerline for a nominal blowing ratio of 1. The coolant jet appears to be mostly attached to the surface, with dimensionless temperatures of ~ 0.5 prevailing in the wake of the jet indicating some level of effectiveness. This is supported by the centerline film effectiveness plotted in Figure 5 for the same nominal blowing ratio of 1. The effectiveness is high at the hole exit and then drops to a fairly consistent level between 0.3 and 0.4 away from the ejection point. Thus the downstream surface temperature is only slightly lower than the downstream jet wake temperature.

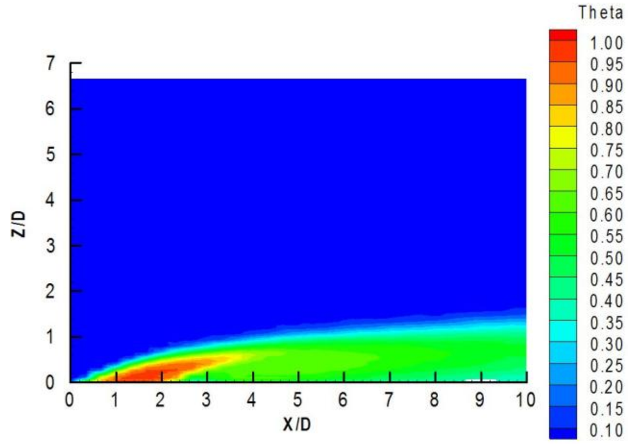

Fig 4. Dimensionless temperature at centerline for M~1

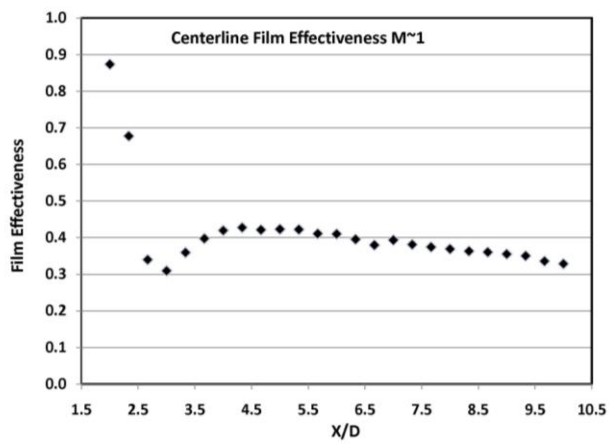

Fig 5. Centerline film effectiveness at M~1

For the case of high blowing ratio (M~2), the centerline temperature contours in Figure 6 suggest that the jet is lifted with temperatures nearly equal to the freestream prevailing near the wall over the entire surface (past a localized cool spot at the jet ejection point).

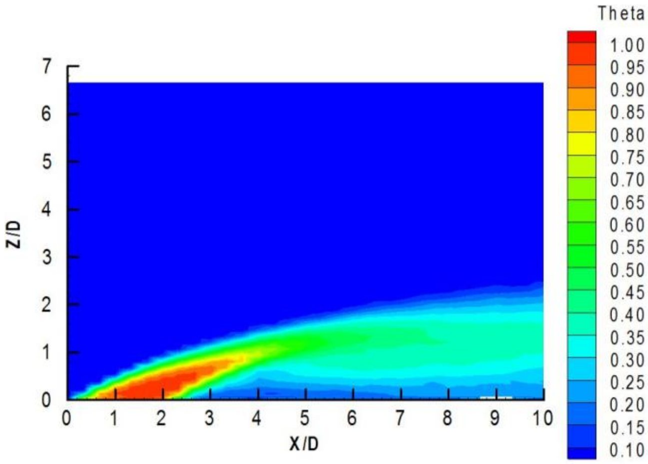

Fig 6. Dimensionless temperature at centerline for M~2

Figure 7 shows the corresponding centerline effectiveness which is low as expected of a detached film jet. The effectiveness (away from the localized peak at the ejection point) is between 0.1 and 0.2 for the high blowing ratio case.

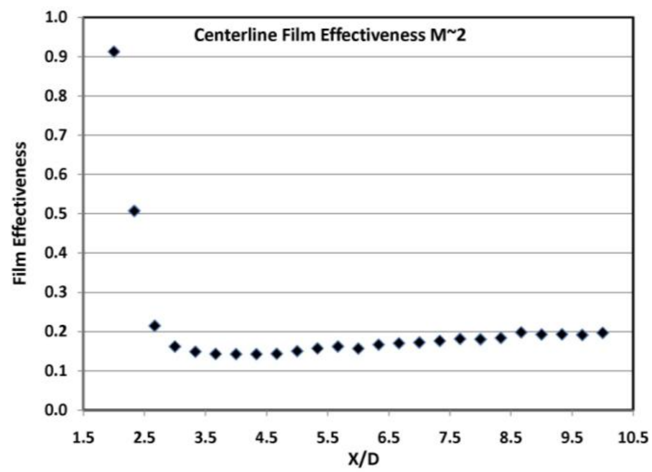

Fig 7. Centerline film effectiveness at M~2

Figure 8 shows the dimensionless temperatures for a blowing ratio of 1 at 5 streamwise locations: x/D of roughly 2, 3, 4, 6, 8 from the leading edge of the film cooling hole. The first location is at the hole trailing edge. It clearly shows the coolant after having been bent by the oncoming mainstream flow. As the coolant moves in the streamwise direction, the dimensionless temperature decreases as the coolant heats up and spreads both in the vertical and spanwise direction. The second image in Figure 8 (at x/D ~3) shows the imprint of a kidney shaped contour due to vortex flows. This shape is lost with the imprint becoming more circular as the jet diffuses moving further downstream.

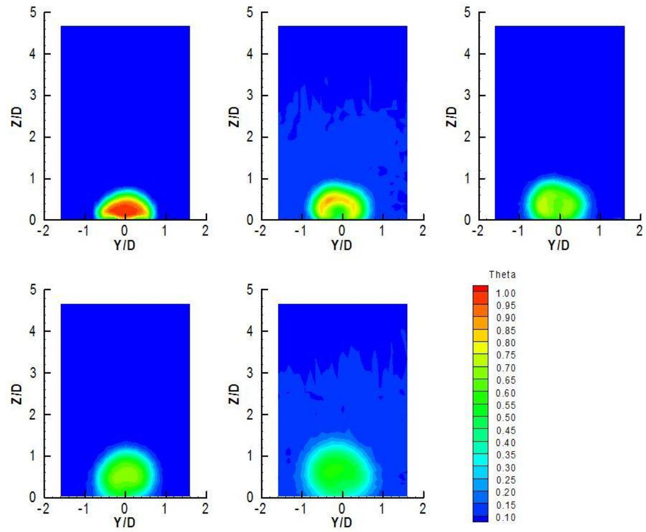

Fig 8. Dimensionless temperatures at streamwise locations x/D~ 2, 3, 4, 6, 8 for M~1

Figure 9 shows the progression of the coolant and freestream thermal interaction for the high blowing ratio case by plotting the dimensionless temperature contours at the same five streamwise locations: approximately 2, 3, 4, 6, 8 hole diameters, D, from the leading edge of the film cooling hole. At the hole trailing edge, the jet core penetrates further away from the wall and the contour appears less flattened than at the same plane at the lower blowing ratio. The second streamwise plane shows a pronounced kidney shape that also appears slightly lifted from the surface. The kidney shape is maintained further downstream as the coolant mixes with the freestream and reduces in temperature. Unlike the lower blowing ratio when the shape of the jet quickly became circular, the higher blowing ratio shape maintains a distinct kidney shape, implying that the counter-rotating vortex pair that is attributed to this shape is stronger at the higher blowing ratio.

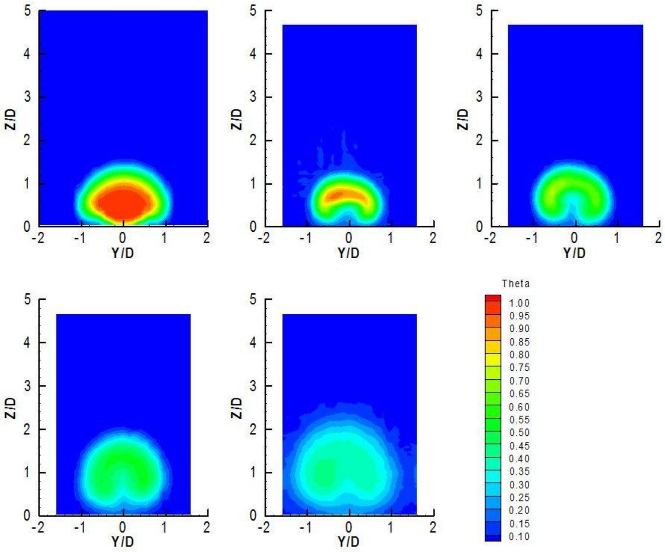

Fig 9. Dimensionless temperatures at streamwise locations x/D~ 2, 3, 4, 6, 8 for M~2

Heat transfer coefficients were calculated based on several different heat flux values from various power supply settings. Figure 10 is a photograph showing a typical color change pattern of the liquid crystal. Such an image represents one heat flux value and there would be multiple heat loads required to obtain a full surface characterization of the heat transfer. Superimposing multiple heat flux levels, it is possible to obtain the full surface heat transfer coefficients from which the Nusselt number distribution can be calculated.

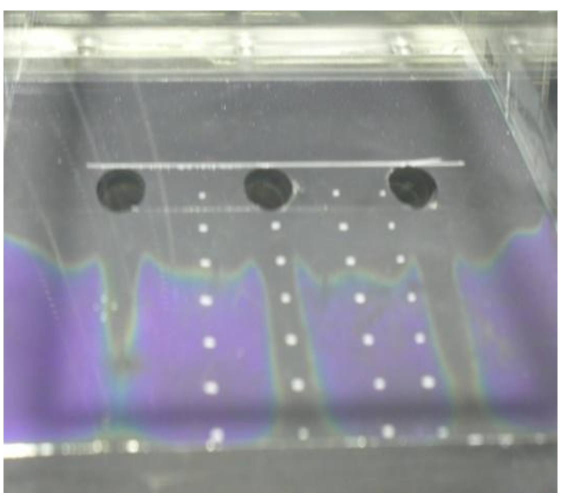

Fig 10. Liquid crystal color pattern for a given heat input

.

Nusselt number distributions are shown for various blowing ratios in Figure 11. Note that these results are for a constant heat flux condition with an unheated starting length before the cooling hole exit plane. Generally for the lower blowing ratios the heat transfer distributions show the coolant jet staying mostly attached and with limited spreading in the spanwise direction. This is similar to the jet spreading seen in the thermal flow field data. Directly behind the hole the effect of the kidney vortex is clearly seen. At the highest blowing ratio, the coolant jet blows off the floor and thus little effect is seen in the heat transfer map; in fact the heat transfer values are similar to a non blowing (M=0) case (not pictured).

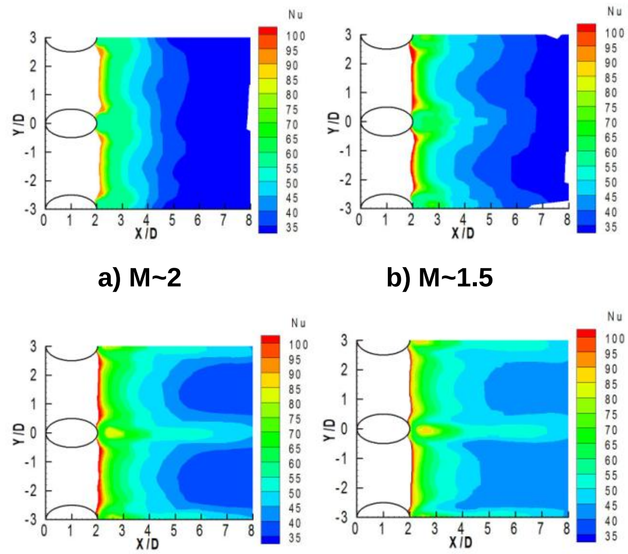

a) M~2 **b) M~1.5**

c) M~1 **d) M~0.5**

Fig 11. Nusselt number distribution for M~2, 1.5, 1, 0.5

Temperature survey data was also taken for the anti-vortex test section. Figure 12 shows temperature profiles at centerline and at dimensionless downstream x/D of 3 and 5. The coolant flow rate at the hole entrance for this case was the same as that for the baseline angled hole with a blowing ratio of 2. Note that since the coolant feed is dispersed through one main and two small exit holes, the exit flow of the main hole is lower in the anti-vortex case relative to the baseline main hole. The significance however is that for the same amount of inlet cooling flow, more surface area is protected by the coolant. The intent of this design is to lessen the strength of the vortex pair which lifts the jet off the surface in the baseline case; the small side jets are meant to counteract the main hole vortex pair. Comparing the anti-vortex model (Figure 12) with the baseline case (Figure 9) we do see that the kidney shape due to those vortices has been greatly reduced and nearly eliminated. Additionally, relative to the baseline case, the center of the jet is closer to the wall in the anti-vortex model; however, this may be a result of the relative lower flow rate from the main hole.

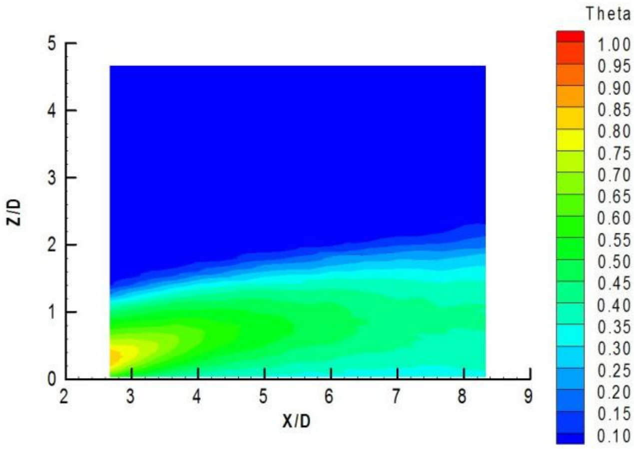

Fig. 12a. Dimensionless temperatures for anti-vortex case at centerline

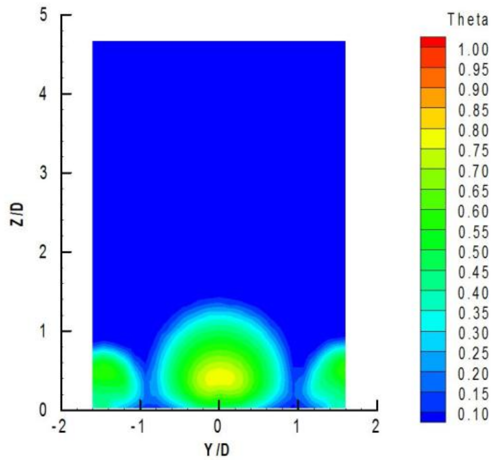

Fig. 12b. Dimensionless temperatures for anti-vortex case at streamwise location x/D=3

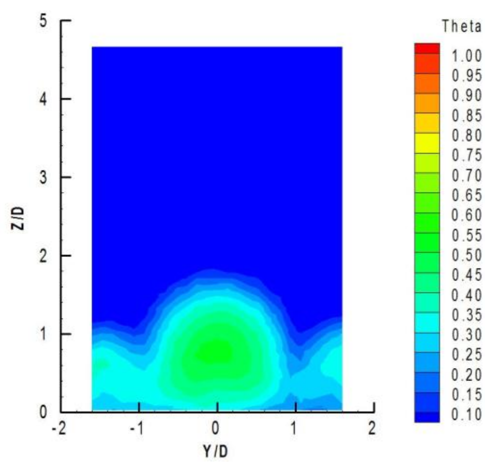

Fig 12c. Dimensionless temperatures for anti-vortex case at streamwise location x/D=5

The film effectiveness is improved for the anti-vortex model relative to the baseline case. Figure 13 shows the span averaged film effectiveness of the anti-vortex model and the baseline model at two downstream locations. Compared to the M~2 baseline case, the anti-vortex model at the same overall coolant flow rate shows improvement of more than twice the baseline. It is also better than M~1 baseline case.

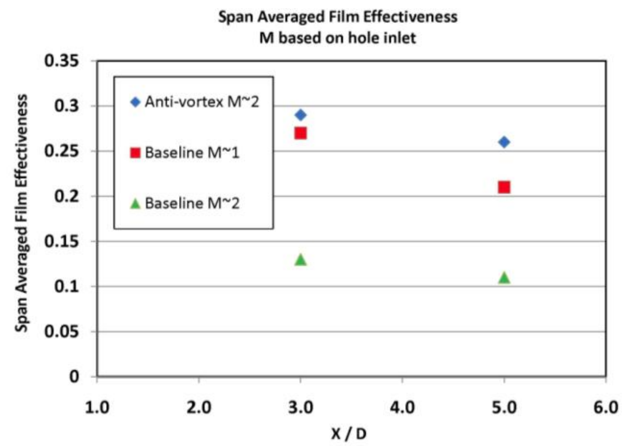

Fig 13. Span averaged film effectiveness

SUMMARY AND CONCLUSIONS

Thermal flow field, surface heat transfer and film effectiveness values were measured for large scale film cooling models at various blowing ratios. Experimental surveys are presented at the centerline of the jet and at various streamwise locations to complement the velocity and turbulence data presented in part 1 of this study. At a blowing ratio of 1, the thermal flow field shows the coolant jet mostly attached to the floor and thus yields a relatively high centerline film effectiveness value of around 0.4. For the blowing ratio of 2 case, the data clearly show the coolant jet lifting off and thus resulting in lower film effectiveness with a centerline value closer to 0.15. The commonly seen kidney shape resulting from uplifting flow vortices is present in the coolant jets at both blowing ratios. Thermal flow field data was also obtained for a modified film cooling model that included angled side jets as an anti-vortex device. The thermal flow data showed a diminished kidney shape and much improved film effectiveness and thus warrants continued study.

ACKNOWLEDGMENTS

The authors would like to acknowledge the support of the NASA Glenn Faculty Fellowship program.

REFERENCES

[1] Leylek, J.H, and Zerkle, R.D., 1994, "Discrete-Jet Film Cooling: A Comparison of Computational Results with Experiments," *Journal of Turbomachinery*, Vol. 116, pp. 358-368.

[2] Walker, D.K., and Leylek, J.H, 1997, "A systematic computational methodology applied to a three-dimensional film-cooling flowfield," *Journal of Turbomachinery*, Vol. 119, pp. 777-785.

[3] El-Gabry, L., Heidmann, J., and Ameri, A., 2010, "Penetration characteristics of film-cooling jets at high blowing ratio," *AIAA Journal*, Vol. 48, pp. 1020-1024.

[4] Thurman, D. T., Poinsatte, P. E. and Heidmann, J. D., 2008, "Heat Transfer Measurements for a Film Cooled Turbine Vane Cascade", ASME paper GT2008-50651, AMSE Turbo Expo 2008, Berlin.

[5] El-Gabry, L.A, Thurman, D.G., Poinsatte, P.E., and Heidman, J.D., 2011, "Turbulence and Heat Transfer Measurements in an Inclined Large Scale Film Cooling Array – Part I, Velocity and Turbulence Measurements," ASME paper GT2011-46491, *ASME Turbo Expo 2011*, Vancouver.

[6] Foster, N.W., and Lampard, D., 1975, "Effect of density and velocity ratio of discrete hole film cooling," *AIAA Journal*, Vol. 113, pp. 1112-1114.

[7] Foster, N.W., and Lampard, D., 1980, "The flow and film cooling effectiveness following injection through a row of holes," *ASME Journal of Engineering for Power*, Vol. 102, pp. 584-588.

[8] Sinha, A.K., Bogard, D.G., and Crawford, M.E., 1991, "Film-Cooling Effectiveness Downtream of a Single Row of Holes with Variable Density Ratio," *Journal of Turbomachinery*, Vol. 113, pp. 442-449.

[9] Kohli, A., and Bogard, D.G., 1997, "Adiabatic effectiveness, thermal fields, and velocity fields for film cooling with large angle injection," *Journal of Turbomachinery*, Vol. 119, pp. 352-358.

[10] Thole, K.A., Sinha, A.K., Bogard, D.G., and Crawford, M.E., 1990, "Mean Temperature Measurements of Jets in Crossflow for Gas Turbine Film Cooling Applications," *Third International Symposium on Transport Phenomena and Dynamics of Rotating Machinery*, Honolulu.

[11] Dhungel, S., Phillips, A., Ekkad, S.V., and Heidmann, J.D., 2007, "Experimental Investigation of a Novel Anti-Vortex Film Cooling Hole Design", ASME paper GT2007-27419, *ASME Turbo Expo 2007*, Montreal.

[12] Yuen, C.H.N., and Martinez-Botas, R.F., 2003, "Film cooling characteristics of a single round hole at various streamwise angles in a crossflow Part II: Heat transfer coefficients," *International Journal of Heat and Mass Transfer*, Vol. 46, pp. 237-249.

[13] Yuen, C.H.N., and Martinez-Botas, R.F., 2005, "Film cooling characteristics of a single round hole at various streamwise angles in a crossflow Part I: Effectiveness," *International Journal of Heat and Mass Transfer*, Vol. 48, pp. 4995-5016.

[14] Goldstein, R.J and Olson, R.L., 1999, "Film cooling effectiveness and mass/heat transfer coefficient downstream of one row of discrete holes," *Journal of Turbomachinery*, Vol. 121, pp 225-232.

[15] Heidmann, J. D., 2008, "A Numerical Study of Anti-Vortex Film Cooling Designs at High Blowing Ratio", ASME paper GT2008-50845, AMSE Turbo Expo 2008, Berlin.

[16] Russell, L., Thurman, D., Simonyi, P.S., Hippensteele, S., Poinsatte, P., 1993, "Measurements and Computational Analysis of Heat Transfer and Flow in a Simulated Turbine Blade Internal Cooling Passage", NASA TM 106189, 1993.